First-order Raman off- and on-resonance scattering induced by F centers in CsCl and CsBr

J. P. Buisson, S. Lefrant, M. Ghomi, and L. Taurel

Laboratoire de Physique Cristalline, Associate Research Group No.13 of the Centre National de la Recherche Scientifique, Université de Paris-Sud, Bâtiment 490, 91405 Orsay Cedex, France

(Received 16 May 1977)

Experimental first-order Raman spectra for CsBr and CsCl doped with F centers are described. All spectra were studied as a function of the wavelength λ_L of the laser line allowing excitation off and on resonance with the F band. Off-resonance spectra were calculated using phonons derived from the eleven-shell model parameters which fit with neutron data, and assuming that the electron-phonon interaction is linear in the displacements of the first- and second-shell ions surrounding the F center. Softening of the longitudinal force constants between the F center and its first nearest-neighbor (nn's) (55% in CsBr, 50% in CsCl) and between its first nn's and its second nn's (8% in CsBr, 13% in CsCl) accounts for the main peaks. The relative contributions of the Γ_1^+, Γ_3^+, Γ_5^+ modes to the 2nd moment of the F band deduced from Raman-scattering cross sections agree with previous magnetic-circular-dichroism measurements. It is shown that in CsBr, F-electron coupling with the first-shell ions is preponderant while in CsCl, the coupling to the Γ_3^+ symmetrized displacements of the second-shell ions appears relatively large.

I. INTRODUCTION

It is well known that when crystals have the CsCl structure, the first-order Raman scattering is forbidden. The introduction of defects, in particular F centers, destroys the translation symmetry of the lattice and the inversion symmetry of all lattice sites except the impurity site itself; therefore, first-order Raman scattering induced by all the perturbed phonons of the first Brillouin zone can be observed.[1-4] The peaks of the spectra reflect the peaks of the perturbed projected densities of one-phonon states for ions which couple to the F center. Then the Raman method is the most detailed experimental source of information about the electron-phonon coupling of the F center. Since the pioneer work done by Worlock and Porto,[5] Raman spectra of F centers in crystals of NaCl structure have been extensively studied in the past,[6-11] but only a preliminary work about Raman scattering in CsBr (F centers) has been recently published.[12] Study of Raman scattering by F centers in cesium halides is very interesting since in these crystals the F-center absorption band is structured at low temperature. In CsBr the F band shows an unresolved doublet, while in CsCl a barely resolved triplet is observed.[13] This structure has stimulated important theoretical work and is now rather well explained.[14-16] The F center has O_h symmetry and the electronic excited state of the F-band transition is a Γ_4^- orbital triplet split by the spin-orbit interaction into a doubly degenerate Γ_6^- and a quadruplet degenerate Γ_8^-. The strong spin-orbit coupling in cesium halides can partially explain a doublet structure as it was first suggested by Margerie *et al.*[17] Moreover, in its excited state the F center suffers a Jahn-Teller interaction due to the coupling to non-cubic-lattice vibrations, which splits the Γ_8^- levels. Therefore, the three-peak structure in CsCl can be explained if the interaction with non-cubic modes is relatively strong with regards to the interaction with the cubic modes.[14] These conclusions were supported by the experimental determination of the cubic- and non-cubic-lattice vibration contributions to the second moment of the F band.[18] Therefore the study of Raman spectra, which shows in detail the coupling to the active modes of each symmetry responsible for the broadening and structure of the F band, is of great interest.

In "off-resonance" excitation conditions, the usual selection rules for first-order Raman scattering show that the active modes have Γ_1^+ (A_{1g}), Γ_3^+ (E_g), and Γ_5^+ (T_{2g}) symmetries.[20] On the other hand, the relative intensities of the experimental Raman peaks must be independent of the exciting light wavelength. In a preliminary work,[12] some Raman spectra of F centers in CsBr have been studied with a tunable dye laser operating in the F absorption band. These spectra exhibit some modifications with the laser-line wavelength, and at that time we have suggested that the changes come from the breaking of the selection rules established in off-resonance excitation. In the present work we have been able to extend the range of the laser-line energy, and also study Raman spectra of CsCl (F centers). All the results confirm that the spectra exhibit dramatic changes when the energy of the laser line operates on resonance with F-band transition, as it was theoretically predicted in the case of F centers in CsF.[21] Calculations based on an extension of Henry's theory[19] show that the spin-orbit coupling of the F center in

its first excited state accounts for the main experimental results.

II. EXPERIMENTAL

A. Experimental details

The homemade CsCl and CsBr samples were taken from monocrystals grown under chlorine and bromine atmosphere by the Bridgman method. The Merck initial product was purified by zone melting.

The F centers were created by γ irradiation at 20°C. After coloration, the samples were stored in the dark to avoid formation of aggregates. In the case of CsBr an additive coloration at 500 °C in potasium vapor was used in order to verify that the spectra do not depend on the coloration method. After coloration, F centers characterized by their absorption band[13,14] are obtained (Fig. 1) and we checked that they are stable under illumination in the F band at 10 K. In CsBr, the F band at 10 K shows two badly resolved peaks F_a and F_b peaking, respectively, at $\lambda_a = 616$ nm (16 234 cm^{-1}) and $\lambda_b = 640$ nm (15 625 cm^{-1}), and in CsCl the F band is formed of three unresolved bands F_a, F_{b_1}, F_{b_2} at $\lambda_a = 558$ nm (17 921 cm^{-1}), $\lambda_{b_1} = 578$ nm (17 301 cm^{-1}), $\lambda_{b_2} = 585$ nm (17 094 cm^{-1}).

The Raman spectra were measured using a Spectra Physics 10-W argon-ion laser in conjunction with a dye cell (Rhodamine 6G or Rhodamine B) allowing the laser-line wavelength to vary within the spectral range 572–662 nm; some spectra were also studied using the 514.5- and 582.7-nm ionized argon emission lines. Then, the study of Raman spectra of the F centers in CsBr, when exciting the whole spectral range of the F band, was possible. Unfortunately, the wavelengths available from the dye laser prevented from observing Raman spectra by excitation in the F_a band (Fig. 1) of CsCl.

The spectra were analyzed with a Spex-model 1401 double monochromator using a 9558 A cooled E.M.I. photomultiplier as receptor. The resolution was about 3 cm^{-1}; all spectra were obtained using the 90° scattering geometries and all samples were oriented using the Lauë back-scattering method.

The experimental geometry of a Raman experiment is denoted by the symbol $\vec{k}_L(\vec{\eta}_L, \vec{\eta}_S)\vec{k}_S$, where $\vec{k}_L, \vec{k}_S$ are, respectively, the propagation directions of the incident and scattered light and where $\vec{\eta}_L$, $\vec{\eta}_S$ denote the unit vectors along the directions of polarization of the incident and scattered light. In our experimental conditions $\vec{k}_L$ and $\vec{k}_S$ were, respectively, parallel to the $[110] = Z$ direction and $[\bar{1}10] = Y$ direction; the $[001]$ direction is denoted by X. Therefore, in off-resonance approximation, the three first-order Raman spectra due to modes of $\Gamma_1^+ + \Gamma_3^+$, Γ_3^+, and Γ_5^+ symmetry can be determined by studying respectively the $Z(XX)Y$, $Z(YZ)Y$, and $Z(YX)Y$ spectra.

Since absolute Raman cross sections have not been measured, Stokes Raman spectra are reproduced (Figs. 2 and 3) in relative value. Then only the intensities of the three spectra observed using the same laser line wavelength can be compared. The frequencies of the Raman peaks ex-

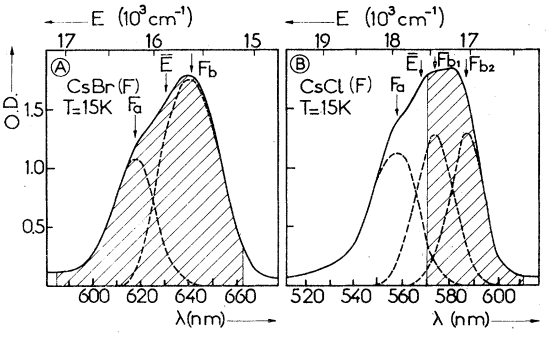

FIG. 1. F-center optical absorption bands at 12 K in CsBr and CsCl. The dashed area shows the spectral range of the dye-laser line used for Raman experiments. (a) CsBr (F centers). Decomposition of the F band into two components (Ref. 17), F_a ($\lambda_a = 616$ nm) and F_b ($\lambda_b = 640$ nm) corresponding to the broadened transitions $\Gamma_1^+ \rightarrow \Gamma_6^-$, $\Gamma_1^+ \rightarrow \Gamma_8^-$ (first moment: $\bar{E} = 15.815\,cm^{-1}$). (b) CsCl ($F$ centers). Decomposition of the F band into three components (Ref. 14), F_a ($\lambda_a = 558$ nm), F_{b_1} ($\lambda_{b_1} = 578$ nm) F_{b_2} ($\lambda_{b_2} = 585$ nm) (first moment: $\bar{E} = 17.250$ cm^{-1}).

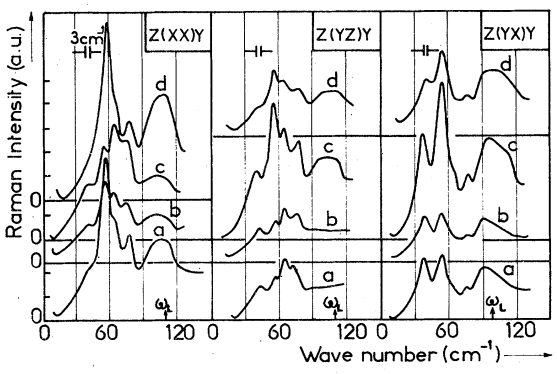

FIG. 2. Stokes Raman spectra of CsBr (F centers) at 12 K for several selected wavelengths λ_L of the laser line; $X = [001]$; $Y = [1\bar{1}0]$; $Z = [\bar{1}10]$; cutoff frequency for phonons (Ref. 23): $\omega_l = 113$ cm^{-1}. (a) $\lambda_L = 650$ nm, (b) $\lambda_L = 640$ nm, (c) $\lambda_L = 625$ nm, (d) $\lambda_L = 600$ nm. In off-resonance approximation the $Z(XX)Y$, $Z(YZ)Y$, and $Z(YX)Y$ geometries give, respectively, the (Γ_1^+, Γ_3^+), Γ_3^+, Γ_5^+ spectra. All spectra were recorded with the same experimental gain. The intensities of the three spectra excited with the same laser-line wavelength can be compared.

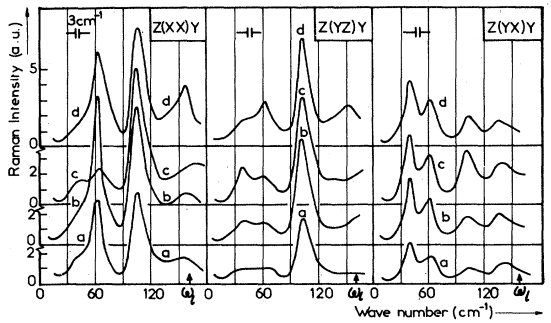

FIG. 3. Stokes Raman spectra of CsCl (F centers) at 12 K for several selected wavelenths λ_L of the laser line; $X=[001]$; $Y=[1\bar{1}0]$; $Z=[110]$; cutoff frequency for phonons (Ref. 24): $\omega_t=162\ \mathrm{cm}^{-1}$. (a) $\lambda_L=610$ nm, (b) $\lambda_L=600$ nm, (c) $\lambda_L=575$ nm, (d) $\lambda_L=528.7$ nm. In off-resonance approximation the $Z(XX)Y$, $Z(YZ)Y$, and $Z(YX)Y$ geometries give, respectively, the $(\Gamma_1^+ + \Gamma_3^+)$, Γ_3^+, and Γ_5^+ spectra. All spectra were recorded with the same experimental gain. The intensities of the three spectra studied with the same laser-line wavelength can be compared.

hibit no significant variations between 10 and 78 K, and their accurate positions (~2 cm^{-1}) were determined at 78 K as average between the Stokes and anti-Stokes peak positions.

At 78 K, a background due to hot fluorescence was superimposed to the spectra, and at 12 K, it decreases. So, we only reproduce the 12-K spectra. In the spectral range of the first-order Raman scattering, corrections due to light absorption and response of the photomultiplier were neglected.

Before coloration, intrinsic second-order Raman spectra, similar to those previously published,[22] were observed at 78 K. After coloration, continuous spectra attributed to F centers appear, and we have verified that in similar experimental conditions, the intrinsic second-order Raman scattering was negligible.

B. Results

1. CsBr (F centers)

Raman spectra were studied as a function of the laser-line wavelength λ_L in the spectral range 580–660 nm. In Fig. 2 are reproduced some typical spectra and Fig. 7 shows the 660-nm spectra, when the exciting photon energy E_L falls at the bottom of the low-energy side of the F band. The previous results[12] are then confirmed: the frequency shifts of the Raman peaks are independent of the exciting wavelength λ_L, but the relative intensities of the peaks in the $Z(XX)Y$, $Z(YZ)Y$, $Z(YX)Y$ spectra strongly depend on λ_L when Raman scattering is on resonance with the F band.

In Table I, the frequency shifts of the main Raman peaks and their symmetry types deduced from the classical selection rules of first-order Raman scattering are indicated for each observation case. The phonon dispersion curves[23] show that the peaks having frequencies lower than 76 cm^{-1} are due to acoustical modes. The phonon cutoff frequency is 113 cm^{-1} in pure crystal, so the broad band at 90–110 cm^{-1} is ascribed to optical modes and also to the superposition of the first- and second-order Raman spectra induced by F centers (see Sec. IV A).

Regarding the variation of the relative intensities of the main Raman peaks, two spectral ranges of the laser light must be distinguished.

(i) $\lambda_L=650$–663 nm. In these conditions, the wavelength λ_L of the laser line falls in the low-energy side of the F band. In this spectral range, the relative intensities of the spectra observed in the three geometry cases, are almost similar whatever the λ_L laser-line wavelength is [Fig. 2, curve a, $\lambda_L=650$ nm; Fig. 8, $\lambda_L=660$ nm]. We may expect that these spectra, in particular the 660-nm spectra, approximates those obtained in off-resonance excitation conditions; hereafter, the 660-nm spectra are denoted as off-resonance

TABLE I. Frequency shifts of first-order Raman peaks in CsBr and CsCl doped with F centers ($T=12$ K). The relative intensities of the peaks are denoted by the following: (F), strong; (f), weak; (m), intermediate; they have been determined from the 660-nm spectra (CsBr, Fig. 8) and the 610-nm spectra (CsCl, Fig. 7).

Observation case	Symmetry of active modes		Peak energy (cm^{-1}) Acoustical modes	Optical modes
$Z(XX)Y$	Γ_1^+, Γ_3^+	CsBr	55 (F) 65 (f) 76 (f)	90–110 (m)
		CsCl	63 (F)	105 (F) 150 (f)
$Z(YZ)Y$	Γ_3^+	CsBr	45 (f) 65 (f) 76 (f)	90–105
		CsCl	40 (f) 70 (f)	105 (F)
$Z(YX)Y$	Γ_5^+	CsBr	39 (m) 55 (m)	90 (f) 100 (f)
		CsCl	39 (m) 63 (m)	100 (f) 140 (f)

spectra. In this case, the usual selection rules of first-order Raman scattering are valid: the spectra taken in the $Z(XX)Y$, $Z(YZ)Y$, and $Z(YX)Y$ geometries are due, respectively, to $\Gamma_1^+ + \Gamma_3^+$, Γ_3^+, and Γ_5^+ modes. The frequency shifts of the peaks are given in Table I: the Γ_1^+ spectrum contains a strong Γ_1^+ band peaking at 55 cm^{-1}, the Γ_5^+ spectrum two bands at 39 and 55 cm^{-1}, and the Γ_3^+ spectrum three very badly resolved bands of low intensity at 45, 65, and 76 cm^{-1}.

(ii) $\lambda_L = 590-650$ nm. In this spectral range, we observe the Raman scattering on-resonance with the F band and in Fig. 2 it is clear (curves b and c) that the relative intensities of the Raman bands exhibit strong changes when λ_L varies; moreover, the breaking of the "usual" selection rules is obvious. Regarding the 55-cm^{-1} peak due to Γ_1^+ phonons two main effects can be discussed. First, the 55-cm^{-1} band appears in the "forbidden" $Z(YZ)Y$ geometry (Fig. 2, curves b,c,d). The ratio ρ between the intensities of the peak measured in the $Z(YZ)Y$ and $Z(XX)Y$ geometries depends on λ_L and has a maximum value for $\lambda_L \simeq 625$ nm. Second, the relative intensity of the 55-cm^{-1} Γ_1^+ peak studied in the $Z(XX)Y$ geometry strongly depends on the laser-line wavelength and becomes particularly low in the 625-nm spectrum (Fig. 2, curve c).

Moreover, as it was previously discussed,[12] the ratio between the intensities of the two bands peaking at 55 and 39 cm^{-1} in the $Z(YX)$ Y geometry reveals some variations as a function of λ_L and reaches a maximum when $\lambda_L \simeq 615$ nm. It is interesting to compare the spectra taken by excitation in the low-energy side ($\lambda_L = 660$ nm: Fig. 2, curve a) and in the high-energy side of the F band ($\lambda_L = 600$ nm: Fig. 2, curve d). The spectra are somewhat similar; however, the anomalies observed in the 600-nm spectra as regards to the 660 nm [55-cm^{-1} Γ_1^+ peak in the $Z(YZ)Y$ spectrum, and the enhancement of the 55-cm^{1} peak in the $Z(YX)Y$ spectrum] are due to the breaking of the selection rules.

2. CsCl (F centers)

Raman spectra were studied within the spectral range 572–620 nm of the laser line wavelength and also using the 528.7-nm laser line. Some typical spectra are reproduced in Fig. 3. In Fig. 7 is shown the 620-nm spectrum, i.e., using excitation in the low-energy side of the F band.

As in the case of the F centers in CsBr, the frequency shifts are independent of λ_L, but the relative intensities of the peaks measured in the three geometries show important variations with λ_L. On the other hand, the 610 and 620-nm spectra are almost similar and we may expect that the 620-nm spectra approximates those obtained in off-resonance excitation.

(a) $\lambda_L = 610-620$ nm. In Table I, the frequency shifts of the main peaks and their symmetry types deduced from the usual selection rules are indicated. The phonon dispersion curves[24] show that the peaks of frequency shifts lower than 87 cm^{-1} are due to acoustical modes. The cutoff frequency of the phonons in pure crystals is 162 cm^{-1} and so, the broad band at 150 cm^{-1} is likely due to the superposition of optical modes and second-order Raman scattering induced by F centers (see Sec. IV A). The two strongest peaks at 63 and 105 cm^{-1} are, respectively, attributed to Γ_1^+ acoustical and to Γ_3^+ optical phonons. The Γ_5^+ spectrum is weaker and mainly contains two peaks at 39 and 63 cm^{-1}.

(b) $\lambda_L = 572-600$ nm; $\lambda_L = 528.7$ nm. When the laser-light wavelength falls into the F band, the breaking of the usual selection rules very clearly appears (Fig. 3, curves b and c). Regarding the 63-cm^{-1} Γ_1^+ peak two main effects can be discussed.

First, the 63-cm^{-1} Γ_1^+ peak appears in the forbidden $Z(YZ)Y$ geometry.

Second, the relative intensity of the 63 cm^{-1} Γ_1^+ peak studied in the $Z(XX)Y$ spectrum exhibits variations when the Raman scattering is in resonance with the F band; in particular, the intensity is very low in the 575-nm spectrum (Fig. 3, curve c).

Moreover, as in the case of CsBr (F centers), the spectra taken by excitation in the high-energy (Fig. 3, curve d: $\lambda_L = 528.7$ nm) and low-energy side of the F band (Fig. 3, curve a: $\lambda_L = 610$ nm) are somewhat similar. However, the breaking of the usual selection rules seen through the depolarization of the 63 cm^{-1} Γ_1^+ mode plays a role in the 528.7-nm spectra.

III. CALCULATIONS IN "OFF-RESONANCE" APPROXIMATION

A. Formalism

Assuming that the incident-photon energy is small compared with any of those for electronic transitions in the perturbed crystals, it was shown[25,26] that the differential Stokes Raman-scattering cross section per unit solid angle Ω per unit frequency ω induced by one F center is given by

$$\left(\frac{d^2\sigma}{d\Omega\, d\omega}\right)_{\vec{\eta}_S,\vec{\eta}_L} = \frac{\omega_L \omega_S^3}{c^4}\,\hbar\,\frac{N_{(\omega)}}{2\omega} \times \sum_{\Gamma,j,r,s}\left(\vec{\eta}_S\cdot\frac{\partial\tilde{\alpha}}{\partial Q^{\Gamma}_{\Gamma,j}}\cdot\vec{\eta}_L\right)\cdot\left(\vec{\eta}_S\cdot\frac{\partial\tilde{\alpha}}{\partial Q^{s}_{\Gamma,j}}\cdot\vec{\eta}_L\right)\rho_{rs}(\omega,\Gamma). \quad (1)$$

TABLE II. Polarizability derivative tensors $\partial\tilde{\alpha}/\partial Q^{r}_{\Gamma,j}$ for the O_h group (Ref. 19).

Γ_1^+	Γ_3^+	Γ_5^+
$\frac{C_1^{(r)}}{(M_r)^{1/2}}\begin{bmatrix}1&0&0\\0&1&0\\0&0&1\end{bmatrix}$	$\frac{C_3^{(r)}}{2(M_r)^{1/2}}\begin{bmatrix}1&0&0\\0&1&0\\0&0&-2\end{bmatrix}$; $\frac{\sqrt{3}C_3^{(r)}}{2(M_r)^{1/2}}\begin{bmatrix}1&0&0\\0&-1&0\\0&0&0\end{bmatrix}$	$\frac{C_5^{(r)}}{(2M_r)^{-1/2}}\begin{bmatrix}0&0&0\\0&0&1\\0&1&0\end{bmatrix}$; $\frac{C_5^{(r)}}{(2M_r)^{-1/2}}\begin{bmatrix}0&0&1\\0&0&0\\1&0&0\end{bmatrix}$; $\frac{C_5^{(r)}}{(2M_r)^{-1/2}}\begin{bmatrix}0&1&0\\1&0&0\\0&0&0\end{bmatrix}$

Here the local-field correction is neglected and the F centers are supposed to be independent. ω_S and ω_L are the frequencies of the scattered and incident radiation; $\vec{\eta}_L$ and $\vec{\eta}_S$ are, respectively, unit vectors along the directions of polarization of the incident and scattered light: $N_{(\omega)} = [1-\exp(-\hbar\omega/k_BT)]^{-1}$ is the Bose factor for the Stokes contribution. $\partial\tilde{\alpha}/\partial Q^{r}_{\Gamma,j}$, $\partial\tilde{\alpha}/\partial Q^{s}_{\Gamma,j}$ are the first-order derivative of the F-center polarizability with respect to the reduced symmetry coordinates $Q^{r}_{\Gamma,j}$ or $Q^{s}_{\Gamma,j}$ transforming according to the jth basis function of the rth or sth representation of Γ type ($\Gamma=\Gamma_1^+,\Gamma_3^+,\Gamma_5^+$). The quantities $\rho_{rs}(\omega,\Gamma)$ are the perturbed normalized projected densities of one phonon states. As usual, they are written in terms of the perturbed Green's function matrix G:[26,27]

$$\rho_{rs}(\omega,\Gamma) = \frac{2\omega}{\pi}\,\mathrm{Im}G_{rs}(\omega,\Gamma), \tag{2}$$

with $G=G^0(I+PG^0)^{-1}$, where G^0 is the Green's function for the perfect crystal and P is a matrix describing the perturbation due to the F center.

The polarizability derivative tensor elements $\partial\tilde{\alpha}/\partial Q_{\Gamma,j}$ are determined by symmetry considerations taken into account the O_h symmetry of the F center.[20] Hereafter the $\partial\tilde{\alpha}/\partial Q_{\Gamma,j}$ elements are written in terms of $C_\Gamma^{(r)}$ parameters defined in Table II, with $C_{\Gamma_1^+}=C_1$, $C_{\Gamma_3^+}=C_3$, $C_{\Gamma_5^+}=C_5$.

The differential cross sections for the three scattering geometries described in Table I are

$$\left(\frac{d^2\sigma}{d\Omega\,d\omega}\right)_{[001],[001]} = K\,\frac{N_{(\omega)}}{2\omega}\times(I_{\Gamma_1^+}+I_{\Gamma_3^+}), \tag{3a}$$

$$\left(\frac{d^2\sigma}{d\Omega\,d\omega}\right)_{[1\bar{1}0],[001]} = K\,\frac{N_{(\omega)}}{2\omega}\times\frac{1}{2}\,I_{\Gamma_5^+}, \tag{3b}$$

$$\left(\frac{d^2\sigma}{d\Omega\,d\omega}\right)_{[1\bar{1}0],[110]} = K\,\frac{N_{(\omega)}}{2\omega}\times\frac{3}{4}I_{\Gamma_3^+}, \tag{3c}$$

with

$$K=\omega_L\omega_S^3\hbar/c^4.$$

The expressions $I_{\Gamma_1^+}, I_{\Gamma_3^+}, I_{\Gamma_5^+}$ depend on the choice of defect space. Two models have been used.

(i) In a rough approximation, we assumed that only the vibrations of the F-center nearest neighbors (i.e., 8 Cs^+) modulate the electronic polariz-

TABLE III. $I_{\Gamma_1^+}$, $I_{\Gamma_3^+}$, $I_{\Gamma_5^+}$ expressions [see formula (3)] in terms of the perturbed projected densities of one-phonon states $\rho_{rs}(\omega,\Gamma)$, where r and s denote the rth or sth representation of Γ type. Line (1): defect space involves the first shell ions. Line (2): defect space involves the first- and second-shell ions. The coefficients $C_\Gamma^{(r)}$ are proportional to $\partial\tilde{\alpha}/\partial Q^{r}_{\Gamma,j}$ defined in Table II. ($m_+=m_{Cs^+}$; $m_-=m_{Cl^-}$ or m_{Br^-}).

$I_{\Gamma_1^+}$	(1)	$\frac{(C_1^{(1)})^2}{m_+}\rho_{11}(\omega,\Gamma_1^+)$
	(2)	$\frac{(C_1^{(1)})^2}{m_+}\rho_{11}(\omega,\Gamma_1^+)+\frac{2C_1^{(1)}C_1^{(2)}}{(m_+m_-)^{+1/2}}\rho_{12}(\omega,\Gamma_1^+)+\frac{(C_1^{(2)})^2}{m_-}\rho_{22}(\omega,\Gamma_1^+)$
$I_{\Gamma_3^+}$	(1)	$\frac{(C_3^{(1)})^2}{m_+}\rho_{11}(\omega,\Gamma_3^+)$
	(2)	$\frac{(C_3^{(1)})^2}{m_+}\rho_{11}(\omega,\Gamma_3^+)+\frac{2C_3^{(1)}C_3^{(2)}}{(m_+m_-)^{+1/2}}\rho_{12}(\omega,\Gamma_3^+)+\frac{(C_3^{(2)})^2}{m_-}\rho_{22}(\omega,\Gamma_3^+)$
$I_{\Gamma_5^+}$	(1)	$\frac{(C_5^{(1)})^2}{m_+}\rho_{11}(\omega,\Gamma_5^+)+\frac{2C_5^{(1)}C_5^{(2)}}{m_+}\rho_{12}(\omega,\Gamma_5^+)+\frac{(C_5^{(2)})^2}{m_+}\rho_{22}(\omega,\Gamma_5^+)$
	(2)	$\frac{(C_5^{(1)})^2}{m_+}\rho_{11}(\omega,\Gamma_5^+)+\frac{(C_5^{(2)})^2}{m_+}\rho_{22}(\omega,\Gamma_5^+)+\frac{(C_5^{(3)})^2}{m_-}\rho_{33}(\omega,\Gamma_5^+)$ $+\frac{2C_5^{(1)}C_5^{(2)}}{m_+}\rho_{12}(\omega,\Gamma_5^+)+\frac{2C_5^{(1)}C_5^{(3)}}{(m_+m_-)^{+1/2}}\rho_{13}(\omega,\Gamma_5^+)+\frac{2C_5^{(2)}C_5^{(3)}}{(m_+m_-)^{+1/2}}\rho_{23}(\omega,\Gamma_5^+)$

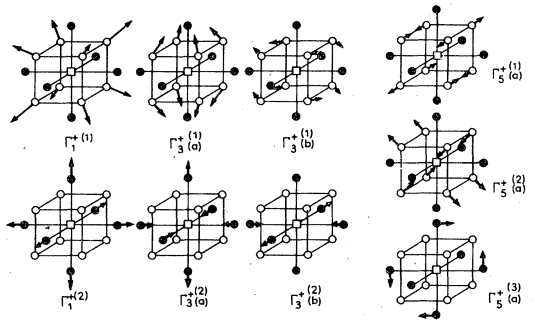

FIG. 4. Displacements of ions in the first- and second-shell ions surrounding the F center in CsCl structure for Γ_1^+, Γ_3^+, Γ_5^+ symmetrized coordinates. Only one partner is represented in the Γ_5^+ motion (F center). ○, Cs^+; ● Cl^- or Br^-.

ability of the F center. In this case, the Raman active symmetry coordinates have $\Gamma_1^+, \Gamma_3^+, \Gamma_5^{+(1)}$, $\Gamma_5^{+(2)}$ symmetries.[22]

(ii) In a more refined model, we have also taken into account the coupling of the F center to the second shell of ions surrounding the F centers (i.e., 6 Cl^- or Br^-). Thus, the defect space has 45 degrees of freedom and the group theory analysis shows that seven symmetry coordinates are Raman active. The $\Gamma_1^{+(1)}, \Gamma_3^{+(1)}, \Gamma_5^{+(1)}, \Gamma_5^{+(2)}$ representations involve symmetrized displacements of the first shell of Cs^+ ions, while the $\Gamma_1^{+(2)}, \Gamma_3^{+(2)}, \Gamma_5^{+(3)}$ representations involve those of the second shell of the Cl^- or Br^- ions. These displacements are represented in Fig. 4, where only one partner of the three dimension Γ_5^+ representations is shown.

In each approximation, the $I_{\Gamma_1^+}, I_{\Gamma_3^+}, I_{\Gamma_5^+}$ expressions are given in Table III.

B. Host-lattice dynamics

The phonon dispersion curves of pure CsBr,[23,28] and pure CsCl,[24] were previously measured by inelastic neutron scattering technique at 80 K. These curves have been calculated[23,24] from phonon frequencies and eigenvectors of the shell model,[29,30] which account for the polarizability of both ions. We have used the same eleven-parameter shell model (model III in Ref. 23, model II in Ref. 24) in order to calculate the phonon density of states of CsBr and CsCl at 80 K. In both crystals we have found that the best parameters which fit the dispersion curves are somewhat different from those published in Refs. 23 and 24 (Table IV).

The total phonon density of states $\rho^0_{(\omega)}$ for the host lattice was calculated for 12 341 wave vectors in the $\frac{1}{48}$ Brillouin zone. The results are in good agreement with previous calculations using a deformation dipole model.[31] The highest frequencies of phonons in CsBr and CsCl are, respectively, 113 and 163 cm^{-1}; in the case of CsCl, a narrow gap exists between 85 and 93 cm^{-1}.

We calculated the projected densities of one-phonon states $\rho^0_{rs}(\omega, \Gamma)$ on the nearest neighbors (8 Cs^+) and second nearest neighbors (6 anions) of the F center using standard methods.[27] Some of the $\rho^0_{rs}(\omega, \Gamma)$ curves giving the most important contributions are shown in Figs. 5 and 6. In the case of CsCl (Fig. 6) the peaks of the densities of one-phonon states projected on the cesium ions occur in the acoustical frequency range while those on the chlorine ions occur in the optical range. Particularly, the curve $\rho^0_{22}(\omega, \Gamma_3^+)$ shows a prominent peak at 115 cm^{-1} due to the Γ_3^+ symmetrized displacements of the first shell of chlorines; this

TABLE IV. Shell-model parameters used in host-lattice dynamics in CsCl and CsBr. Parameters are defined in Refs. 22 and 23. Units: e, electron charge; v, volume of the unit cell.

		CsBr		CsCl	
Parameters	Units	Present work	Rolandson and Raunio [a]	Present work	Ahmad et al. [b]
A_{12}	$e^2/2v$	7.99	8.39	8.0	7.863
B_{12}	$e^2/2v$	−0.29	−0.29	−0.149	0
A_{11}	$e^2/2v$	0.78	0.97	1.039	0.702
B_{11}	$e^2/2v$	−0.14	−0.22	−0.421	−0.121
A_{22}	$e^2/2v$	0.20	0.20	−0.147	0.663
B_{22}	$e^2/2v$	0.22	0.12	0.098	−0.163
Z	e	0.849	0.849	0.884	0.821
α_1	Å^3	1.10	0.51	2.807	1.477
α_2	Å^3	1.32	1.72	2.808	2.361
d_1	e	−0.040	−0.08	−0.04	0.088
d_2	e	0.040	0.044	0.037	0.087
Lattice parameter	Å	4.240		4.088	

[a] Reference 23.
[b] Reference 24.

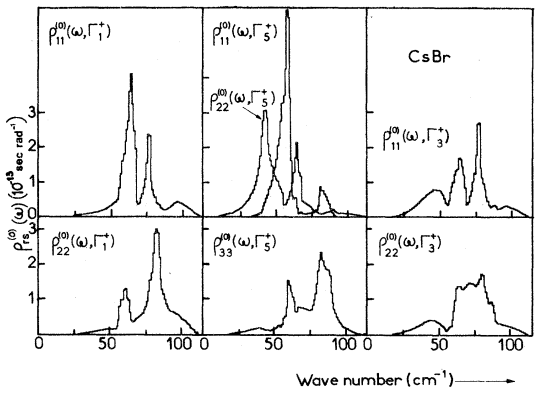

FIG. 5. Histogram of the projected densities of one-phonon states for unperturbed phonons of Γ_1^+, Γ_3^+, and Γ_5^+ symmetry type in CsBr (F centers) (width of each bin: $\Delta\omega = 1$ cm^{-1}). Above: projection on the first-shell ions surrounding an F center. Below: projection on the second-shell ions surrounding an F center. Histograms were computed using an eleven-parameter shell model (Ref. 23) at 78 K. (Parameter values, see Table IV.)

effect comes from the low ratio of mass between chlorine and cesium ions ($m_{Cl^-}/m_{Cs^+} = 0.267$). On the other hand, in the case of CsBr, cesium and bromine ions contribute both to the projected densities of states in the acoustical and optical ranges.

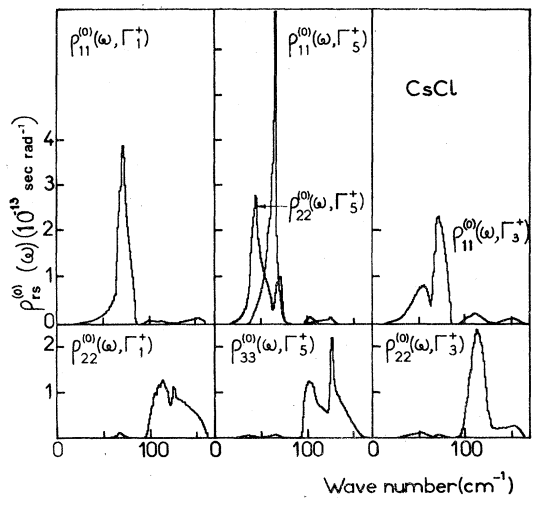

FIG. 6. Histogram of the projected densities of one phonon states for unperturbed phonons of Γ_1^+, Γ_3^+, and Γ_5^+ symmetry type in CsCl (F centers) (width of each bin: 1 cm^{-1}). Above: projection on the first-shell ions surrounding an F center. Below: projection on the second-shell ions surrounding an F center. Histograms were compared using an eleven-parameter shell model (Ref. 24) at 78 K. (Parameter values, see Table IV.)

C. Perturbation matrix

The perturbation matrix P was expressed in terms of the variations of the force constants (see Appendix). We only took into account the changes δk_{01l} and δk_{12l} in the longitudinal force constants A_{12} between the F center and its first nn's and between its first nn's and its second nn's since all other force constants are much lower (Table IV). Then using relations (2) and (3) and Table III, the differential Stokes Raman cross sections can be calculated in relative value for several values of the $\mu_1 = \delta k_{01l}/A_{12}$ and $\mu_2 = \delta k_{12l}/A_{12}$ parameters.

D. Results

Our purpose is to determine the best set of parameters (i.e., $C_\Gamma^{(r)}$, μ_1, and μ_2) which fit to the Raman spectra studied in off-resonance condition. The frequencies of the first-order Raman peaks reflect the maxima of the perturbed projected densities of one-phonon states $\rho_{rs}(\omega, \Gamma)$ which mainly depend on the force constant perturbations; then, the experimental frequencies of the prominent peaks allow to determine the best set of parameters μ_1 and μ_2. Since the spectra, except the background, do not significantly vary between 12 and 78 K, the use of the shell-model parameters determined at 78 K is justified. The differential cross sections given by the formula (3) have been expressed in terms of the ratios $C_\Gamma^{(r)}/C_1^{(1)}$ which then can be determined to account for relative intensities of the Raman peaks. This method, i.e., first determining the force constant perturbations via peak positions and then determining the $C_\Gamma^{(r)}$ relative value via relative peak intensities, was justified, since we have verified *a posteriori* that the crossed projected densities of one phonon states give small contributions to the Raman scattering. The independent set of parameters $C_\Gamma^{(r)}$, μ_1, and μ_2 used to account for each spectra are indicated in Table V.

TABLE V. Relative values of the $C_\Gamma^{(r)}$ parameters which express the polarizability derivative tensor with regards to the symmetrized displacements of the first- and second-shell ions. Two possibilities for $C_5^{(2)}/C_5^{(1)}$ ratio values fit experimental $Z(YX)Y$ spectrum: ($C_1^{(2)} = 0$, $C_5^{(3)} = 0$). μ_1 and μ_2 are the relative changes in the longitudinal force constant between the F center and its first nn's and its second nn's.

	$\left\lvert\frac{C_3^{(1)}}{C_1^{(1)}}\right\rvert$	$\frac{C_3^{(2)}}{C_3^{(1)}}$	$\left\lvert\frac{C_5^{(1)}}{C_1^{(1)}}\right\rvert$	$\frac{C_5^{(2)}}{C_5^{(1)}}$	μ_1	μ_2
CsBr	0.75	0.25	0.8	0.6	−0.55	−0.08
CsCl	0.45	2	0.9	0.8	−0.50	−0.13
			0.7	−1.45		

1. CsCl (F centers)

When the electron-phonon coupling of the F center is restricted to the first nn's (i.e., 8 Cs^+ ions), a strong disagreement occurs as regards to the strong 105-cm^{-1} peak of Γ_3^+ symmetry (Fig. 7, $Z(YZ)Y$ spectrum). Indeed, in this model of perturbation, the Stokes Raman differential cross section $(d^2\sigma/d\Omega d\omega)_{[1\bar{1}0],[110]}$ involves only the projected density of states $\rho_{11}(\omega, \Gamma_3^+)$ (Table III) which is independent of the change of the longitudinal force constants, and depends only slightly on a modification of the transverse force constant.

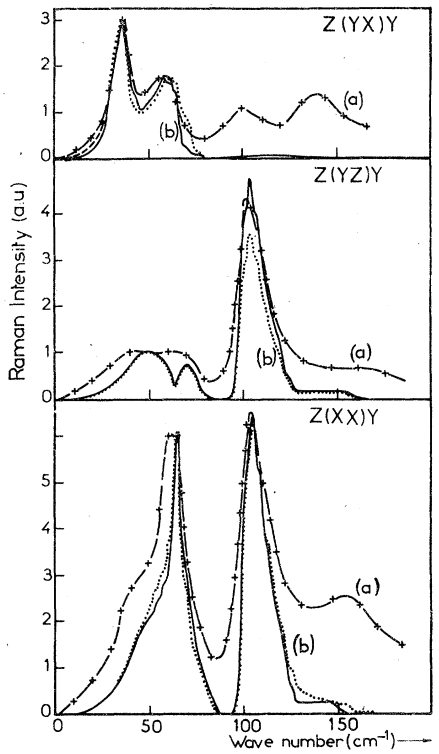

FIG. 7. Experimental and calculated first-order Stokes Raman spectra of CsCl (F centers) at $T = 12$ K for $\lambda_L = 620$ nm (a) Experimental spectra taken in the $Z(XX)Y$, $Z(YZ)Y$, and $Z(YX)Y$, and $Z(YX)Y$ geometries. $X = [001]$; $Y = [1\bar{1}0]$; $Z = [110]$. All spectra were recorded with the same experimental gain. (b) Calculated spectra in off-resonance approximation for a 50% and a 13% decrease in the longitudinal force constants between the F center and its first nn's and between last ones and its second nn's, respectively. Two sets of $C_\Gamma^{(r)}$ values (for definition see Table II) have been used. $Z(YX)Y$ geometry: full line: $|C_5^{(1)}/C_1^{(1)}| = 0.9$, $C_5^{(2)}/C_5^{(1)} = 0.8$, $C_5^{(3)} = 0$; dotted line: $|C_5^{(1)}/C_1^{(1)}| = 0.7$, $C_5^{(2)}/C_5^{(1)} = -1.46$, $C_5^{(3)} = 0$. $Z(YZ)Y$ and $Z(XX)Y$ geometries: full line: $C_1^{(2)} = 0$, $|C_3^{(1)}/C_1^{(1)}| = 0.45$, $C_3^{(2)}/C_3^{(1)} = 2$; dotted line: $C_1^{(2)}/C_1^{(1)} = 1$, $|C_3^{(1)}/C_1^{(1)}| = 0.45$, $C_3^{(2)}/C_3^{(1)} = 1.8$. The calculated spectra have been normalized to reflect the experimental intensity for the 39-cm^{-1} $\Gamma_5^{+(2)}$ peak in the $Z(YX)Y$ spectrum.

Therefore, with a good approximation $(d^2\sigma/d\Omega d\omega)_{[1\bar{1}0],[110]}$ remains proportional to $(1/m^*)(C_3^{(1)})^2\rho_{11}^0(\omega, \Gamma_3^+)$. Since the $\rho_{11}^0(\omega, \Gamma_3^+)$ function has no peaks within the optical frequency range (Fig. 6), this simple model of perturbation is unable to account for the Γ_3^+ spectrum.

In the model of perturbation extended to the second neighbors, the Γ_3^+ spectrum involves the perturbed projected density of one-phonon states $\rho_{22}(\omega, \Gamma_3^+)$, which depends on the modification of the longitudinal force constants; In pure crystals, $\rho_{22}^0(\omega, \Gamma_3^+)$ has a strong peak at 115 cm^{-1} (Fig. 6) and we can expect that the coupling of the F center with the second-shell ions accounts for the 105-cm^{-1} strong peak of Γ_3^+ symmetry.

The μ_1 and μ_2 parameter values have been determined to fit the strong Γ_1^+ (63 cm^{-1}) and Γ_3^+ (105 cm^{-1}) peaks. A good agreement between calculated and experimental frequencies was obtained with reasonable μ_1 and μ_2 values: $\mu_1 = -0.5$, $\mu_2 = -0.13$ (Fig. 7). Moreover, using these values, the 39 and 63-cm^{-1} Γ_5^+ peaks are perfectly reproduced; they are especially due to the $\Gamma_5^{+(2)}$ (39 cm^{-1}) and $\Gamma_5^{+(1)}$ (63 cm^{-1}) types of modes involving the displacements of the first-shell ions. As it could be expected the motion of the second shell ions only slightly affect the Γ_5^+ spectrum since the $Q_{\Gamma_5^+}^{(3)}$ symmetrized displacements (Fig. 4) of the Cl^- ions are perpendicular to the axis joining the F center and each Cl^- ion.

The relative intensities of the spectra allow to determine the coupling parameters $C_\Gamma^{(r)}$ with relative value. The Γ_3^+ and $(\Gamma_1^+ + \Gamma_3^+)$ spectra were calculated with $C_1^{(2)}/C_1^{(1)} = 1$ or 0. In each case, the best sets of parameters $|C_3^{(1)}/C_1^{(1)}|$, $C_3^{(2)}/C_3^{(1)}$ was determined to fit the experimental spectra (Fig. 7, curve a). The results are weakly modified when the coupling of the F center to the Γ_1^+ displacements of the second-shell ion is taken into account. The main result is the strong coupling to the Γ_3^+ displacements of the second-shell ions. Indeed, in each hypothesis, the $|C_3^{(2)}/C_1^{(1)}|$ ratio is about 0.9, while the $|C_3^{(1)}/C_1^{(1)}|$ ratio is about 0.45. In order to calculate the Γ_5^+ spectrum, the coupling to the Γ_5^+ displacements of the second-shell ions was neglected. Two sets of parameters: $C_5^{(2)}/C_5^{(1)} = 0.8$ and $C_5^{(2)}/C_5^{(1)} = -1.45$ fit the experimental spectra (Fig. 7) within the frequency-shift range 0–70 cm^{-1}.

2. CsBr (F centers)

We made analogous calculations to reproduce the experimental Raman spectra. The position of the main peaks, in particular the 55-cm^{-1} Γ_1^+ mode, the 39 and the 55-cm^{-1} Γ_5^+ modes are in good agreement with the calculated ones with $\mu_1 = -0.55$ and

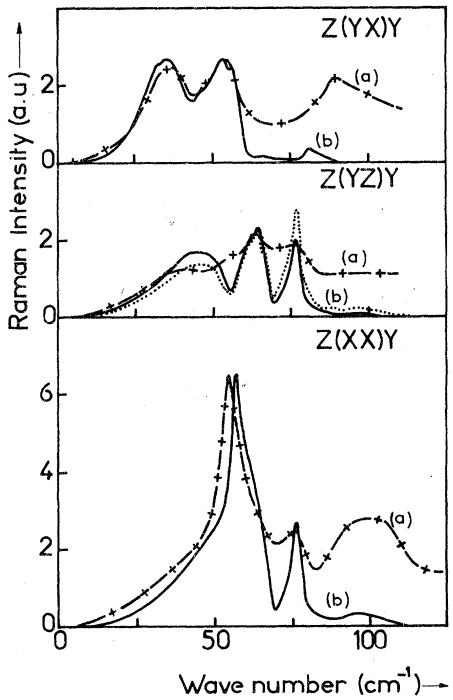

FIG. 8. Experimental and calculated first-order Stokes Raman spectra of CsBr (F centers) at $T=12$ K for $\lambda_L=660$ nm. (a) Experimental spectra taken in the $Z(XX)Y$, $Z(YZ)Y$, and $Z(YX)Y$ geometries. $X=[001]$; $Y=[1\bar{1}0]$; $Z=[110]$. All spectra were recorded with the same instrumental gain. (b) Calculated spectra in off-resonance approximation for a 55% and a 8% decrease in the longitudinal force constants between the F center and its first nn's and between last ones and its second nn's, respectively. $Z(YX)Y$ geometry: $|C_5^{(1)}/C_1^{(1)}|=0.8$, $C_5^{(2)}/C_5^{(1)}=0.6$. $Z(YZ)Y$ and $Z(XX)Y$ geometries: dotted line: $C_1^{(2)}=C_3^{(2)}=0$, $|C_3^{(1)}/C_1^{(1)}|=0.8$; full line: $C_1^{(2)}=0$, $C_3^{(2)}/C_3^{(1)}=0.25$, $|C_3^{(1)}/C_1^{(1)}|=0.75$. The calculated spectra have been reproduced to reflect the experimental intensity for the 55-cm^{-1} $\Gamma_5^{(1)}$ peak in the $Z(YX)Y$ spectrum.

$\mu_2=-0.08$ (Fig. 8). As regards the $C_\Gamma^{(r)}$ parameters, we neglected the variations of the F center polarizability due to the Γ_5^+ and Γ_1^+ displacements of the second shell of ions, i.e., we put $C_5^{(3)}=C_1^{(2)}=0$; these approximations are justified since, as in the case of CsCl, the spectra only slightly depend on the displacements of the second shell of anions in these types of motions. Spectra due to Γ_3^+ modes were reproduced with $C_3^{(2)}=0$ and $C_3^{(2)}\neq 0$ [Fig. 8(b) 8(b): $Z(YZ)Y$ and $Z(XX)Y$ spectra]; although the spectra are somewhat similar, the results are improved when the coupling of the F center with the Br^- ions is taken into account. The comparison between calculated and experimental spectra shows that the best agreement occurs with $|C_3^{(1)}/C_1^{(1)}|=0.75$; $C_3^{(2)}/C_3^{(1)}=0.25$ (Fig. 8).

IV. DISCUSSION AND CONCLUSION

A. Off-resonance Raman spectra

1. CsCl (F centers)

The comparison between experimental and calculated spectra (Fig. 7) shows the good agreement between the predicted and experimental frequency shifts of the main peaks (39, 63, and 105 cm^{-1}), using a softening of the longitudinal force constants between the F center and its 1 nn's ($\mu_1=-50\%$) and between its first nn's and second nn's ($\mu_2=-13\%$); these changes in the interionic force constants are very analogous to those previously obtained in the case of F centers in crystals of NaCl structure.[6,11,32] As it was shown, the 63 and 105-cm^{-1} peaks of the $Z(XX)Y$ spectrum are ascribed to the coupling of the F center, respectively, to the Γ_1^+ displacements of the first shell and to the $\Gamma_3^{+(2)}$ displacements of the second-shell ions. The 39- and 63-cm^{-1} peaks of the $Z(YX)Y$ spectrum mainly come from the prominent peaks at 45 and 65 cm^{-1} in the projected densities of one-phonon states of the host lattice: respectively, $\rho_{22}^0(\omega,\Gamma_5^+)$ and $\rho_{11}^0(\omega,\Gamma_5^+)$ (Fig. 6). These 45- and 65-cm^{-1} frequency shifts decrease with the softening of the interionic longitudinal force constants, thus, the 39- and 63-cm^{-1} peaks of Γ_5^+ symmetry are due to the coupling of the F center with, respectively, the $\Gamma_5^{+(2)}$ and $\Gamma_5^{+(1)}$ displacements of the first-shell ions.

However, the most important result is the evidence of a strong coupling of the F center with the Γ_3^+ type displacements of the first anion shell (second-shell ions); indeed, the ratio between the coefficients $C_3^{(2)}$ and $C_1^{(1)}$ is about 0.9 (Table V). This effect has been predicted and discussed previously by Moran,[14] who has qualitatively shown that, in this type of motion, the $\Gamma_3^{+(a)}$ symmetrical coordinates (Fig. 4) of the halogens enhance the variation of the electrostatic potential caused by $\Gamma_3^{(a)}$ displacements of the Cs^+ ions: the degree of enhancement depends on the relative amplitude of the halogen vibrations, which happens to be large in the case of the light chlorines ($m_{Cl^-}/m_{Cs^+}=0.267$).

In the high-frequency optical range, the calculated first-order Raman spectra very strongly disagree with the experimental ones; this partly comes from the superposition of the second-order Raman scattering induced by F centers. The second-order spectra were previously discussed, especially in the case of F centers in NaBr,[33] and KI.[11] The origin of the three main broad bands at 100 and 140 cm^{-1} in the $Z(YX)Y$ spectrum, at 150 cm^{-1} in the $Z(XX)Y$ and $Z(YZ)Y$ spectra may be qualitatively explained from harmonics and

TABLE VI. Contributions of the cubic and noncubic modes to the second moment of the F band ($\langle M_2\rangle_{nc} = \langle M_2\rangle_3 + \langle M_2\rangle_5$).

	$(\langle M_2\rangle_3/\langle M_2\rangle_1)^{1/2}$	$(\langle M_2\rangle_5/\langle M_2\rangle_1)^{1/2}$	$(\langle M_2\rangle_{nc}/\langle M_2\rangle_1)^{1/2}$ Present work	Henry *et al.*[a]
CsCl	1.50	1.48	2.10	2.09
CsBr	0.82	1.06	1.34	1.33

[a] Reference 18.

combination sums of the 63 (Γ_1^+), 105 (Γ_3^+), 39 (Γ_5^+), and 63(Γ_5^+) modes, using the second-order selection rules. It is not the purpose of this paper to discuss the second-order spectra; we just want to note that the superposition of first- and second-order spectra, particularly in the shift frequency range 78–126 cm^{-1}, can affect the determination of the ratio $C_3^{(2)}/C_3^{(1)}$. However, a rough evaluation of the second-order scattering contribution shows that the error is lower than 10%.

It is well known,[19] that in off-resonance conditions, the first-order Raman scattering cross sections can be related to the several contributions $\langle M_2\rangle_1$, $\langle M_2\rangle_3$, and $\langle M_2\rangle_5$ in the second moment $\langle M_2\rangle$ of the F band. Since the second-order Raman scattering prevents the accurate knowledge of the first-order spectra in the high-optical frequency range, we used the calculated spectra (Fig. 7, curves b) to determine the relative values of each second moment of the F band. The results (Table VI) show that the contribution of the noncubic modes is about twice that of the cubic modes; this is in very good agreement with previous determinations of $\langle M_2\rangle_1$ and $\langle M_2\rangle_3 + \langle M_2\rangle_5$ by magnetic circular dichroism method,[18] though it seems purely fortuitous since measurements are not very accurate.

2. CsBr (F centers)

A softening of the longitudinal force constants between the F center and its first nn's ($\mu_1 = -55\%$) and between its first nn's and second nn's ($\mu_2 = -8\%$) explains the frequency shifts of the main peaks. The prominent peak at 55 cm^{-1} in the $Z(XX)Y$ spectrum is principally due to the coupling of the F center with the Γ_1^+ displacements of the first-shell ions. In the $Z(YX)Y$ spectrum the two peaks at 39 and 55 cm^{-1} originates from the $\Gamma_5^{+(2)}$ and $\Gamma_5^{+(1)}$ displacements of the first-shell, respectively. On the other hand, in the $Z(YZ)Y$ spectrum, the broad bands at 45, 55, and 76 cm^{-1} originates from the Γ_3^+ displacements of the first- and second-shell ions. The relative intensities of the main peaks are rather well explained when using the $C_\Gamma^{(r)}$ adjustable parameters reported in Table V. As in the case of CsCl, the agreement between experimental and calculated spectra improves when the coupling of the F center with Γ_3^+ displacements of the bromine ions is taken into account; however, as we could expect, since $m_{Br^-}/m_{Cs^+} \simeq 0.60$ and $m_{Cl^-}/m_{Cs^+} \simeq 0.267$, this coupling is considerably lower in the case of F centers in CsBr than in CsCl.

The disagreement between experimental and calculated spectra in the shift-frequency range 80–113 cm^{-1} (Fig. 8) can be partly attributed to a harmonic of the strong 55-cm^{-1} Γ_1^+ mode and additive combinations of the 55-cm^{-1} Γ_1^+ mode with Γ_3^+ and Γ_5^+ modes.

Table VI indicates the calculated contribution of each type of motion to the second moment of the F band in relative value; as in the case of CsCl (F centers) the results confirm those previously obtained from magnetic circular dichroism method.[18]

B. Raman spectra on resonance with the F band

As it was shown in Sec. II, Raman spectra induced by F centers exhibit very strong changes when the laser line is tuned out of the F band into the F-band region. The breaking of the conventional selection rules is particularly clear in the case of the main peaks due to the Γ_1^+ modes [i.e.,: 55-cm^{-1} peak in CsBr (F) and 63-cm^{-1} peak in CsCl (F)]; indeed, these modes give rather important contributions to the first-order Raman spectra taken in the usual forbidden $Z(YZ)Y$ and $Z(YX)Y$ geometries (Figs. 2 and 3). On the other hand, as regards the Γ_3^+ modes, in particular the 105-cm^{-1} peak in CsCl (F), no strong anomalies of polarization were observed. Similar results remain valid for the $\Gamma_5^{+(2)}$ modes responsible for the 39-cm^{-1} peaks in CsCl (F) and CsBr (F); we are thus allowed to assume that this is also valid for the $\Gamma_5^{+(1)}$ modes which give the 55-cm^{-1} peak in CsBr (F) and the 63-cm^{-1} peak in CsCl (F) spectra taken in the $Z(YX)Y$ geometry and in off-resonance condition. Therefore, the relative variations of intensity, as a function of the laser-line wavelength λ_L, of the 55-cm^{-1} [CsBr (F)] and the 63-cm^{-1} [CsCl (F)] peaks in the $Z(YX)Y$ spectra must be ascribed to the depolarization of the 55-

and 63-cm^{-1} Γ_1^+ modes, as it was previously suggested in a preliminary study of Raman scattering by F centers in CsBr.[12]

Another important result is the strong dependence between λ_L and the relative intensities of the spectra induced by Γ_1^+ modes, taken in the $Z(XX)Y$ geometry. This effect very clearly appears in the case of the 55-cm^{-1} Γ_1^+ peak in CsBr (F) spectra (Fig. 2). A systematic study has shown that this peak has a very special low intensity compared to that of the Γ_3^+ peaks when $\lambda_L \simeq 625$ nm (Fig. 2, curve c).

Our purpose is now to explain the unusual behavior of the first-order Raman scattering on resonance with the F band, in particular the spectra of CsBr (F) since a systematic study of the spectra when varying λ_L in the whole region of the F band has been made. Let us remind that recent experimental results about Raman scattering studied in quasi-resonance with the F band in KI (F) have stressed the breakdown of the usual selection rules proved by the depolarization of the Γ_1^+ resonant mode.[7,11] At that time, it was only suggested and then justified[34] that the spin-orbit coupling of the F center in its first excited state was responsible for this effect. Moreover, recent calculations of resonant Raman scattering led to similar conclusions.[35]

Previously, a resonant Raman theory[36] including the F-center radiative damping, which properly takes the electron-phonon interaction to infinite order, has been developed; recently this formalism was extended to take into account the F-electron spin.[21] In the present paper we have used simple calculations in order to explain the main features of the resonant experimental spectra of CsBr (F). Further calculations of the CsBr (F) spectra showed that both methods can interpret the experimental results.[37] The semiclassical theory of Raman scattering discussed by Henry[19] in the case of the quasi-resonance was extended to the case of resonance. This theory uses the expression of the electronic polarizability[25] which, of course, is not valid when the incident photon energy is on resonance with an electronic transition. Nevertheless, it was pointed out[38] that this expression can be used to explain some features of the resonance spectra if the lifetime τ of the excited state is taken into account. This lifetime includes the radiative damping of the electronic oscillator and the damping of the vibrations of the nuclei due to vibrational relaxation[39] when the F center is in its first excited state. Then, in the case of light excitation in the F band, the differential Stokes Raman cross section for polarization direction $\vec{\eta}_S$ and $\vec{\eta}_L$ can be written as

$$\left(\frac{d^2\sigma}{d\Omega\, d\omega}\right)_{\vec{\eta}_L,\vec{\eta}_S} = \frac{\omega_L \omega_S^3}{C^4}\ \mathrm{av}_a \sum_{a' \neq a} \left| \sum_b \frac{\langle a' | M\vec{\eta}_S | b\rangle\langle b | M\vec{\eta}_L | a\rangle}{E_b - E_a - E_L + \frac{1}{2} i\gamma} \right|^2 \delta\left(\frac{E_a - E_{a'}}{\hbar} - \omega\right). \tag{4}$$

Here av_a denotes an average over the initial states a; $|a\rangle$ and $|b\rangle$, are, respectively, the initial and intermediate states having E_a and E_b energies; $|a'\rangle$ is the final state, E_L is the energy of incident photon. The damping factor γ is supposed to be independent of the intermediate state. The Hamiltonian H of the system (F electron plus lattice) is taken as[18,19]

$$H = H_E + H_{so} + H_{latt.} + H_{e\text{-}ph}$$

where H_e is the Hamiltonian of the F electron neglecting spin-orbit coupling and with the lattice fixed at $Q = 0$ when the F-center electron is in its orbital ground state $|\alpha\rangle$. This Hamiltonian has eigenstates $|\alpha\rangle|m\rangle$, and $|\beta_i\rangle|m\rangle$, ($|\beta_i\rangle = |x\rangle, |y\rangle, |z\rangle$; $|m\rangle = |+\frac{1}{2}\rangle$ or $|-\frac{1}{2}\rangle$). Here we only retain transitions giving rise to the F band since in our experimental conditions, the transitions responsible for K and L bands are supposed to give negligible contributions to the electronic polarizability. H_{so} describes the spin-orbit interaction which splits the Γ_4^- excited state into a doublet Γ_6^- and a quadruplet Γ_8^- states. $H_{latt.}$ describes the lattice vibrations in the harmonic approximation and has eigenstates $|l\rangle$ of E_l energies. $H_{e\text{-}ph}$ is an electron-phonon coupling term taken as linear in the reduced symmetrical coordinates $Q^{\gamma}_{\Gamma,j}$ which couple to the F excited electronic states in the adiabatic approximation. The main approximation[18,19] is that $H_{e\text{-}ph}$ and H_{so} only mix the $|\beta_i\rangle|m\rangle$ states with each other and that $|\alpha\rangle|m\rangle$ remains unaffected. In this approximation, the only modes which couple to the F center have Γ_1^+, Γ_3^+, and Γ_5^+ types of symmetry. Then, the ground and final states $|a\rangle, |a'\rangle$ are written as Born-Oppenheimer products $|a\rangle = |\alpha\rangle|m\rangle|l\rangle$, $|a'\rangle = |\alpha\rangle|m'\rangle|l'\rangle$, while the $|b\rangle$ excited states are taken as linear combinations of Born-Oppenheimer products $|\beta_i\rangle|m\rangle|l\rangle$, which diagonalize the H Hamiltonian.

The differential angular Raman cross section can be written as

$$\left(\frac{d^2\sigma}{d\Omega\, d\omega}\right)_{\vec{\eta}_S,\vec{\eta}_L} = \frac{\omega_L \omega_S^3}{C^4}\ \mathrm{av}_l \times \sum_{l' \neq l}\ \mathrm{av}_m \sum_m\ |\langle l'|P^{m'm}_{\vec{\eta}_S,\vec{\eta}_L}|l\rangle|^2 \times \delta\left(\frac{E_{l'}-E_l}{\hbar} - \omega\right), \tag{5}$$

where $P^{m'm}_{\vec{\eta}_S,\vec{\eta}_L}$ is the electronic polarizability operator given by

$$P^{m'm}_{\vec{\eta}_S,\vec{\eta}_L} = \sum_b \frac{\langle m'|\langle\alpha|M_{\vec{\eta}_S}|b\rangle\langle b|M_{\vec{\eta}_L}|\alpha\rangle|m\rangle}{E_b - E_a - E_L + \frac{1}{2}i\gamma}\ . \tag{6a}$$

Since the $|b\rangle$ states are eigenstates of the H Hamiltonian we can write

$$\frac{1}{E_b - E_a - E_L + \frac{1}{2}i\gamma} = \langle b|\ \frac{1}{\overline{E} + H_{so} + H_{latt} - E_l + H_{e\text{-}ph} - E_L + \frac{1}{2}i\gamma}\ |b\rangle \tag{6b}$$

(here the relation $E_b - E_a = \langle b|\overline{E} + H_{so} + H_{e\text{-}ph} + H_{latt} - E_l|b\rangle$ was used[18]).

In Plazeck's approximation (same notations as in Sec. II A)

$$\left(\frac{d^2\sigma}{d\Omega\, d\omega}\right)_{\vec{\eta}_S,\vec{\eta}_L} = \frac{\omega_L\omega_S^3}{C^4}\,\hbar\,\frac{N_{(\omega)}}{2\omega}\sum_\Gamma\sum_j\sum_r\sum_s \mathrm{av}_m \sum_{m'}\left(\frac{\partial P^{m'm}_{\vec{\eta}_S\vec{\eta}_L}}{\partial Q^r_{\Gamma,j}}\right)^*_0\left(\frac{\partial P^{m'm}_{\vec{\eta}_S\vec{\eta}_L}}{\partial Q^s_{\Gamma,j}}\right)_0 \rho_{rs}(\Gamma,\omega)\,, \tag{7}$$

where the electronic polarizability is taken as linear in the reduced symmetrical coordinates.

In this approximation, the first derivatives of the electronic polarizability are calculated at the equilibrium position of the ions surrounding the F center. In the case of resonant excitation, Condon's approximation can be used, so the modulation of the electronic polarizability only comes from the variation of the denominator under vibrations of the F center neighboring ions. In the two last approximations, only the purely electronic transitions are considered; in order to take into account for the whole set of virtual states, we have associated an effective damping factor γ^* to each electronic transition. Calculations of the differential scattering cross sections given by (7) become easy when taking into account the relation between A and B operators: $(1/A = 1/B + 1/B \times (B-A)1/A = 1/B + 1/B(B-A)1/B + \cdots)$, where $B - A = -H_{e\text{-}ph}$. The second term (linear in $Q^r_{\Gamma,j}$), in agreement with Eq. (7), is the only one which is taken into consideration.

Then (6a) becomes

$$P^{m'm}_{\vec{\eta}_S\vec{\eta}_L} = -f^2\sum_i\sum_j \langle m'|\langle\beta_{\vec{\eta}_S}|\ \frac{1}{\overline{E} - E_L + H_{so} + \frac{1}{2}i\gamma^*}\ |\beta_i\rangle\langle\beta_i|H_{e\text{-}ph}|\beta_j\rangle\langle\beta_j|\ \frac{1}{\overline{E} - E_L + H_{so} + \hbar\omega + \frac{1}{2}i\gamma^*}\ |\beta_{\vec{\eta}_L}\rangle|m\rangle\,, \tag{8}$$

with

$$f^2 = |\langle\alpha|M_z|z\rangle|^2.$$

From (7) and (8), the differential cross sections for first-order Raman scattering (Stokes process) are easily obtained for each geometry polarizations. For example, we give their expressions in formula (9a), (9b), and (9c) when the Raman scattering is induced by the Γ_1^+ displacements of the first-shell ions, and when we write

$$H_{e\text{-}ph} = \frac{1}{\sqrt{m_+}}\ V_1^{(1)} Q_{\Gamma_1^+}\,,$$

$$\left(\frac{d^2\sigma}{d\Omega\, d\omega}\right)^{(\Gamma_1^+)}_{[001],[001]} = K\left(\frac{N_{(\omega)}}{2\omega}\right) \times \frac{1}{9}\left|\frac{2}{u(u+\omega)} + \frac{1}{v(v+\omega)}\right|^2 \times (\overline{E} - E_L)^4 I_{\Gamma_1^+}\,, \tag{9a}$$

$$\left(\frac{d^2\sigma}{d\Omega\, d\omega}\right)^{(\Gamma_1^+)}_{[1\bar{1}0],[110]} = K\left(\frac{N_{(\omega)}}{2\omega}\right) \times \frac{1}{9}\left|\frac{1}{u(u+\omega)} - \frac{1}{v(v+\omega)}\right|^2 \times (\bar{E}-E_L)^4 I_{\Gamma_1^+}\,, \tag{9b}$$

$$\left(\frac{d^2\sigma}{d\Omega\, d\omega}\right)^{(\Gamma_1^+)}_{[1\bar{1}0],[001]} = \left(\frac{d^2\sigma}{d\Omega\, d\omega}\right)^{(\Gamma_1^+)}_{[1\bar{1}0],[110]}\,, \tag{9c}$$

with

$$K = \frac{\omega_L \omega_S^3 \hbar}{C^4}\,\pi\,,$$

$$I_{\Gamma_1^+} = \frac{(A_1^{(1)})^2 f^4}{(\bar{E}-E_L)^4}\,\frac{\rho_{11}}{m_+}\,(\omega,\Gamma_1^+)\,, \tag{10}$$

$$u = \bar{E}-E_L+\frac{\Delta^*}{3}+\frac{i\gamma}{2}\,,$$

$$v = \bar{E}-E_L-\frac{2\Delta^*}{3}+\frac{i\gamma}{2}\,.$$

The $A_1^{(1)}$ electron-phonon coupling parameter expresses the matrix elements of the $V_1^{(1)}$ operator calculated on the $|x\rangle$, $|y\rangle$, $|z\rangle$ basis.

Since Plazeck's approximation was used, Jahn-Teller interactions due to electron coupling with the noncubic modes are neglected. It is known that, in the case of F centers in CsBr, this effect mainly leads to a repulsion of the Γ_8^- and Γ_6^- levels[14]; therefore, in a phenomenological point of view, the use of an effective spin-orbit coupling energy Δ^* appears more convenient. This Δ^* value can be approximatively calculated:

$$\Delta^* \simeq -\left[\Delta^2 + 3(\langle M_2\rangle_3 + \langle M_2\rangle_5)\right]^{1/2}$$

with

$$(\langle M_2\rangle_3 + \langle M_2\rangle_5)^{1/2} = 289\ \text{cm}^{-1}$$

and $\Delta = -333\ \text{cm}^{-1}$ (Ref. 18), the Δ^* value is about $-600\ \text{cm}^{-1}$.

Moreover, it is obvious that, in Condon's approximation, the $C_\Gamma^{(r)}$ coefficients deduced from first-order Raman spectra taken in off-resonance condition (Table V) are proportional to the electron-phonon coupling parameters which express the matrix elements of $H_{e\text{-}ph}$ electron-phonon Hamiltonian. Indeed, when $(\bar{E}-E_L)/|\Delta^*| > 1$ the depolarization ratio

$$\left(\frac{d^2\sigma}{d\Omega\, d\omega}\right)^{(\Gamma_1^+)}_{[1\bar{1}0],[110]} \Big/ \left(\frac{d^2\sigma}{d\Omega\, d\omega}\right)^{(\Gamma_1^+)}_{[001],[001]}$$

is lower than 10%, then, the usual selection rules are almost valid, as it was shown in the 660-nm spectra. In this case

$$\left(\frac{d^2\sigma}{d\Omega\, d\omega}\right)^{(\Gamma_1^+)}_{[001],[001]} \simeq K\,\frac{N_{(\omega)}}{2\omega}\,I_{\Gamma_1^+}\,. \tag{11}$$

In such a case the comparison between $I_{\Gamma_1^+}$ expressions given in (10) and Table III (first line) shows that the electron-phonon coupling parameter $A_1^{(1)}$ is related to $C_1^{(1)}$ by

$$A_1^{(1)} = \frac{(\bar{E}-E_L)^2}{f^2}\,C_1^{(1)}\,.$$

Similar relations hold for electron-phonon coupling parameter $A_\Gamma^{(r)}$, which can then be deduced in relative value from the $C_\Gamma^{(r)}$ coefficients given in Table V.

Using $\Delta^* = -600\ \text{cm}^{-1}$ we calculated the ratio of the Γ_1^+ and Γ_3^+ mode contributions to Raman spectra in the $Z(XX)Y$ geometry. This ratio depends on the incident photon energy E_L and exhibits a minimum value (independent of γ^*) for $E_L \simeq 16\,058\ \text{cm}^{-1}$ ($\lambda_L \simeq 623$ nm), very close to the experimental one ($\lambda_L \simeq 625$ nm). The spectra calculated for several values of the γ parameter show that the best fit between theoretical and experimental spectra is obtained when $\gamma^* \simeq 650\ \text{cm}^{-1}$. As an example, experimental and calculated spectra are shown in Fig. 9 when $\lambda_L = 625$ nm. Though the relative intensities of the peaks are not very accurately reproduced, the main features of the spectra are on the contrary well interpreted: a strong 55-cm^{-1} peak due to Γ_1^+ modes appears in the usual forbidden $Z(YZ)Y$ and $Z(YX)Y$ geometries, whereas this peak disappears in the spectrum taken in the usual allowed $Z(XX)Y$ geometry. This effect is due to interferences between contributions of the Γ_8^- and Γ_6^- states, as it is clearly revealed in formulas (9a) and (9b). Moreover, calculations show that the spectra due to Γ_3^+ and Γ_5^+ modes almost follow the usual selection rules in agreement with the resonant experimental spectra. The 55-cm^{-1} peak in the $Z(YX)Y$ spectrum is effectively due both to the $\Gamma_5^{+(1)}$ modes and to the depolarization of the 55-cm^{-1} Γ_1^+ mode; calculations allow us to determine in this spectrum the ratio of intensity of the 55- and 39-cm^{-1} peaks as a function of the laser-line wavelength, this ratio has a maximum value for $\lambda_L \simeq 615$ nm in agreement with experiment. Therefore, this semiclassical theory explains rather well the main features of Raman spectra in resonance with the F band in CsBr. Moreover, this theory also explains why

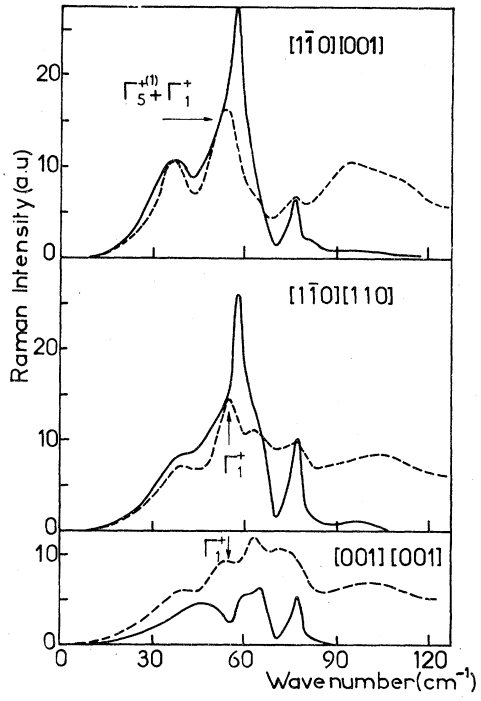

FIG. 9. Experimental and theoretical Raman spectra of CsBr (F centers) under excitation in F band (λ_L = 625 nm) at 12 K for incident and scattered polarization directions: [1$\bar{1}$0]→[001], [110]→[1$\bar{1}$0], [001]→[001]. Dashed line: experimental spectra. All spectra were recorded with the same experimental gain. In optical range, second-order Raman spectra of F centers are superimposed to the first-order spectra. Full line: theoretical first-order Stokes Raman spectra calculated with: $\mu_1 = -0.55$, $\mu_2 = -0.08$, $C_1^{(2)} = 0$, $|C_3^{(1)}/C_1^{(1)}| = 0.75$, $C_3^{(2)}/C_3^{(1)} = 0.25$, $|C_5^{(1)}/C_1^{(1)}| = 0.8$, $C_5^{(2)}/C_5^{(1)} = 0.6$. The calculated spectra have been reproduced to reflect the experimental intensity for the 39-cm^{-1} $\Gamma_5^{+(2)}$ peak in the [1$\bar{1}$0]→[001] spectrum.

the breaking of the usual selection rules with respect to the Γ_1^+ modes remains important when the wavelength of the exciting light falls in the high energy of the F band (Fig. 2, curve d). Indeed the variation of the depolarization ratio ρ as a function of λ_L predicts a ρ value about 40% when $\lambda_L = 600$ nm. This theory does not explain the enhancement of the scattering due to electron interaction with the longitudinal optic modes of high frequency [see Fig. 2(d), 90–110-cm^{-1} frequency range] and observed in the $Z(XX)Y$ geometry; this effect likely comes from the excitation of higher-energy F-center transitions and was recently discussed to explain the changes of the spectra in KCl (F) when the laser line is tuned from the F band to the K band.[40]

Earlier, the depolarization ratio ρ of the Γ_1^+ resonant mode observed in the Raman spectra of F centers in KI[11] was studied in quasi-resonance conditions and interpreted from the relation $\rho = 4\Delta^2/9(E_L - E)^2$. This relation is an approximation of the ρ value determined from formulas (9a) and (9b), almost valid in our experimental conditions; however, the ρ measurements allowed to determine only a Δ^* effective value, and this can explain the disagreement between the Δ value obtained by circular magnetic dichroism experiments and deduced from the depolarization of the resonant mode.

In conclusion, the spectra taken in resonance with the F band in CsBr are rather well explained when the spin-orbit coupling of the F center, is taken into account, which splits the first Γ_4^- excited orbital state into Γ_6^- and Γ_8^- states,, is taken into account, and when an effective value Δ^* of the spin-orbit energy is used. The breaking of the usual selection rules is particularly important in the case of Γ_1^+ modes, which contributes to the Raman scattering in the three geometry polarizations [001]→[001]; [110]→[1$\bar{1}$0]; [1$\bar{1}$0]→[001].

Moreover, the Raman scattering induced by interactions between the Γ_6^- and Γ_8^- electronic states with the Γ_1^+ phonons exhibits interference effects. This explains the variations of the Γ_1^+ Raman peak intensities when the laser-line wavelength is varying within the whole region of the F band.

APPENDIX: DEFECT-MATRIX CALCULATIONS

The space of the P defect matrix is restricted to the F center, its eight nearest-neighbor cations, and its six nearest-neighbor anions. We express the P matrix in terms of the variations δk_{01l}, δk_{01t}, δk_{02l}, δk_{02t}, δk_{12l}, δk_{12t}, δk_{11l}, and δk_{11t} of the parameters of the used-shell model, A_{12}, B_{12}, A_{22}, B_{22}, A_{12}, B_{12}, A_{11}, and B_{11}, respectively (Table IV), where A refers to the longitudinal force constant and B to the transverse force constant. The suffixes 0, 1, and 2 in the δk_{ij} terms refers, respectively, to the F center, a cation of the first-ion shell, and an anion of the second-ion shell: for instance, δk_{01l} is the variation of the longitudinal force constant A_{12} between the F center and a cation of the first-ion shell.

We first write down the general expressions of the $P(\Gamma)$ matrix for the Raman active Γ_1^+, Γ_3^+, Γ_5^+ symmetrical displacements of ions surrounding the F center:

$$P(\Gamma_1^+)=\begin{bmatrix} \frac{1}{m_+}\left(\delta k_{01l}+\frac{1}{3}\,\delta k_{12l}+\frac{8}{3}\,\delta k_{12t}+2\delta k_{11l}\right) & \frac{1}{(m_+m_-)^{1/2}}\,\frac{2}{3}\,(\delta k_{12l}-4\delta k_{12t}) \\ \frac{1}{(m_+m_-)^{1/2}}\,\frac{2}{3}\,(\delta k_{12l}-4\delta k_{12t}) & \left(\frac{1}{m_-}\,\delta k_{02l}+\frac{4}{3}\,(\delta k_{12l}+2\delta k_{12t})\right) \end{bmatrix}$$

$$P(\Gamma_3^+)=\begin{bmatrix} \frac{1}{m_+}\left(\delta k_{01t}+\frac{4}{3}\,\delta k_{12l}+\frac{5}{3}\,\delta k_{12t}+2\delta k_{11l}\right) & -\frac{1}{(m_+m_-)^{1/2}}\,\frac{2}{3}\,(2\delta k_{12l}+\delta k_{12t}) \\ -\frac{1}{(m_+m_-)^{1/2}}\,\frac{2}{3}\,(2\delta k_{12l}+\delta k_{12t}) & \frac{1}{m_-}\left(\delta k_{02l}+\frac{4}{3}\,(\delta k_{12l}+\delta k_{12t})\right) \end{bmatrix} \tag{A1}$$

$$P(\Gamma_5^+)=\begin{bmatrix} \frac{1}{m_+}\left(\frac{1}{3}\,(\delta k_{01l}+2\delta k_{01t})+(\delta k_{12l}+2\delta k_{12t})+2(\delta k_{11l}+2\delta k_{11t})\right) & \frac{1}{m_+}\,\frac{\sqrt{2}}{3}\,[(\delta k_{01l}-\delta k_{01t})-(\delta k_{12l}-\delta k_{12t})] & \frac{1}{(m_+m_-)^{1/2}}\,\frac{2\sqrt{2}}{3}\,(\delta k_{12l}-\delta k_{12t}) \\ \frac{1}{m_+}\,\frac{\sqrt{2}}{3}\,[(\delta k_{01l}-\delta k_{01t})-(\delta k_{12l}-\delta k_{12t})] & \frac{1}{m_+}\left(\frac{1}{3}\,(2\delta k_{01l}+\delta k_{01t})+\frac{1}{3}\,(2\delta k_{12l}+7\delta k_{12t})+2\delta k_{11t}\right) & \frac{1}{(m_+m_-)^{1/2}}\,2\delta k_{12t} \\ \frac{1}{(m_+m_-)^{1/2}}\,\frac{2\sqrt{2}}{3}\,(\delta k_{12l}-\delta k_{12t}) & \frac{1}{(m_+m_-)^{1/2}}\,2\delta k_{12t} & \frac{1}{m_-}\left(\frac{4}{3}\,(\delta k_{12l}+2\delta k_{12t})+\delta k_{02t}\right) \end{bmatrix}$$

Since the longitudinal force constant A_{12} is of an order of magnitude higher than the others, we have only taken into account the δk_{01l} and δk_{12l} variation. Then, in Raman spectra calculations, we used the $P(\Gamma)$ matrices

$$P(\Gamma_1^+)=\begin{bmatrix} \frac{1}{m_+}\left(\delta k_{01l}+\frac{1}{3}\,\delta k_{12l}\right) & \frac{1}{(m_+m_-)^{1/2}}\,\frac{2}{3}\,\delta k_{12l} \\ \frac{1}{(m_+m_-)^{1/2}}\,\frac{2}{3}\,\delta k_{12l} & \frac{1}{m_-}\,\frac{4}{3}\,\delta k_{12l} \end{bmatrix},$$

$$P(\Gamma_3^+)=\begin{bmatrix} \frac{1}{m_+}\,\frac{4}{3}\,\delta k_{12l} & -\frac{1}{(m_+m_-)^{1/2}}\,\frac{4}{3}\,\delta k_{12l} \\ -\frac{1}{(m_+m_-)^{1/2}}\,\frac{4}{3}\,\delta k_{12l} & \frac{1}{m_-}\,\frac{4}{3}\,\delta k_{12l} \end{bmatrix}, \tag{A2}$$

$$P(\Gamma_5^+)=\begin{bmatrix} \frac{1}{m_+}\left(\frac{1}{3}\,\delta k_{01l}+\delta k_{12l}\right) & \frac{1}{m_+}\,\frac{\sqrt{2}}{3}\,(\delta k_{01l}-\delta k_{12l}) & \frac{1}{(m_+m_-)^{1/2}}\,\frac{2\sqrt{2}}{3}\,\delta k_{12l} \\ \frac{1}{m_+}\,\frac{\sqrt{2}}{3}\,(\delta k_{01l}-\delta k_{12l}) & \frac{1}{m_+}\,\frac{2}{3}\,(\delta k_{01l}+\delta k_{12l}) & 0 \\ \frac{1}{(m_+m_-)^{1/2}}\,\frac{2\sqrt{2}}{3}\,\delta k_{12l} & 0 & \frac{1}{m_-}\,\frac{4}{3}\,\delta k_{12l} \end{bmatrix}.$$

[1]D. A. Kleinman, Phys. Rev. 134, A423 (1964).
[2]A. A. Maradudin, in *Solid State Physics*, edited by F. Seitz and D. Turnbull (Academic, New York, 1966), Chap. XIX, p. 1.
[3]G. Benedek and G. F. Nardelli, Phys. Rev. 154, 837 (1968).
[4]T. P. Martin, J. Phys. C 5, 493 (1972).
[5]J. M. Worlock and S. P. S. Porto, Phys. Rev. Lett. 15, 697 (1965).
[6]C. J. Buchenauer, D. B. Fitchen, and J. B. Page, Jr., in *Proceedings of the International Conference of Light Scattering, New York, 1968,* edited by G. B. Wright (Springer-Verlag, New York, 1969), p. 521.
[7]J. P. Buisson, A. Sadoc, L. Taurel, and M. Billardon, in *Light Scattering in Solids*, edited by M.Balkanski, R. C. C. Leite, and S. P. S. Porto (Flammarion, Paris, 1975), p. 587.
[8]A. Sadoc, J. P. Benoit, and L. Taurel, in Ref. 7, p. 593.
[9]D. S. Pan and F. Lüty, in Ref. 7, p. 540.
[10]J. P. Buisson, M. Ghomi, and L. Taurel, Solid State Commun. 8, 407 (1970).
[11]J. P. Buisson, S. Lefrant, A. Sadoc, L. Taurel, and M. Billardon, Phys. Status Solidi B 78, 779 (1976).
[12]S. Lefrant, J. P. Buisson, and L. Taurel, C. R. Acad. Sci. B 282, 407 (1976).
[13]H. Rabin and J. H. Schulman, Phys. Rev. 120, 2007 (1960).
[14]P. R. Moran, Phys. Rev. 137, A1016 (1965).
[15]D. B. Fitchen, Phys. Rev. 133, A1599 (1964).
[16]K. Cho, J. Phys. Soc. Jpn. 25, 1372 (1968).
[17]J. Margerie and R. Romestain, C. R. Acad. Sci. B 258, 4490 (1964).
[18]C. H. Henry, S.E. Schnatterly, and C. P. Slichter, Phys. Rev. 137, A583 (1965).
[19]C. H. Henry, Phys. Rev. 152, 699 (1966).
[20]L. Couture and J. P. Mathieu, Ann. Phys. (Paris) 3, 521 (1948).
[21]E. Mulazzi and M. F. Bishop, J. Phys. Colloq. C7, 1 (1976).
[22]B. S. Agrawal, R. D. Kirby, and J. R. Hardy, Phys. Rev. B 11, 5153 (1975).
[23]S. Rolandson and G. Raunio, Phys. Rev. B 4, 4617 (1971).
[24]A. A. Z. Ahmad, H. G. Smith, N. Wakabayashi, and M. K. Wilkinson, Phys. Rev. B 6, 3956 (1972).
[25]M. Born and K. Huang, *Dynamical Theory of Crystal Lattices* (Oxford U.P., London, 1954), Chap. 4.
[26]A. A. Maradudin, Ref. 2, p. 19 (see also references of previous work in this review article).
[27]G. P. Montgomery, M. V. Klein, B. N. Ganguly, and R. F. Wood, Phys. Rev. B 6, 4047 (1972).
[28]J. Daubert, Phys. Lett. 32A, 437 (1970).
[29]A. D. B. Woods, W. Cochran, and B. N. Brockhouse, Phys. Rev. A 119, 980 (1960).
[30]E. R. Cowley and D. Okazaki, Proc. R. Soc. Lond. A 300 (1967).
[31]B. S. Agrawal and J. R. Hardy, Solid State Commun. 14, 239 (1974).
[32]G. Benedek and E. Mulazzi, Phys. Rev. 179, 906 (1969).
[33]G. Benedek and E. Mulazzi, *Proceedings of the International Conference of Light Scattering, New York, 1968,* edited by G. B. Wright (Springer-Verlag, Berlin, 1969), p. 531.
[34]M. Billardon, M. F. Russel, J. P. Buisson, and S. Lefrant, J. Phys. (Paris) 37, 251 (1976).
[35]E. Mulazzi and N. Terzi, Solid State Commun. 18, 721 (1976).
[36]V. Hizhyakov and I. Tehver, Phys. Status Solidi 21, 755 (1967).
[37]J. P. Buisson and E. Mulazzi, International Conference on Lattice Dynamics, Paris, 1977 (to be published).
[38]V. Weiskopf, Z. Phys. 85, 451 (1933).
[39]P. P. Shorygin, Sov. Phys. Usp. 99 (1973).
[40]D. Robbins and J. B. Page, Phys. Rev. Lett. 38, 365 (1977).